Atmos. Chem. Phys. Discuss., 13, 20165–20194, 2013
www.atmos-chem-phys-discuss.net/13/20165/2013/
doi:10.5194/acpd-13-20165-2013

Atmospheric Chemistry and Physics Discussions

Projections of atmospheric mercury levels and their effect on air quality in the United States

H. Lei[1,2], D. J. Wuebbles[2], X.-Z. Liang[3], Z. Tao[4], S. Olsen[2], R. Artz[1], X. Ren[1], and M. Cohen[1]

[1]National Oceanic and Atmospheric Administration (NOAA), Air Resources Laboratory, College Park, Maryland, USA
[2]Department of Atmospheric Sciences, University of Illinois, Urbana, Illinois, USA
[3]Department of Atmospheric and Oceanic Science, and Earth System Science Interdisciplinary Center, University of Maryland, College Park, Maryland, USA
[4]Universities Space Research Association/NASA Goddard Space Flight Center, Greenbelt, Maryland, USA

Received: 13 June 2013 – Accepted: 18 July 2013 – Published: 2 August 2013

Correspondence to: H. Lei (hang.lei@noaa.gov)

Published by Copernicus Publications on behalf of the European Geosciences Union.

Abstract

The individual and combined effects of global climate change and emissions changes from 2000 to 2050 on atmospheric mercury levels in the US are investigated by using the global climate-chemistry model, CAM-chem, coupled with a mercury chemistry-physics mechanism (CAM-Chem/Hg). Three future pathways from the Intergovernmental Panel on Climate Change (IPCC) Special Report on Emissions Scenarios (SRES) are considered, with the A1FI, A1B and B1 scenarios representing the upper, middle and lower bounds of potential climate warming, respectively. The anthropogenic and biomass burning emissions of mercury are projected from the energy use assumptions in the IPCC SRES report. Natural emissions from both land and ocean sources are projected using dynamic schemes. The zonal mean surface total gaseous mercury (TGM) concentrations in the tropics and mid-latitudes of the Southern Hemisphere are projected to increase by 0.5–1.2 ng m^{-3} in 2050. TGM concentration increases are greater in the low latitudes than they are in the high latitudes, indicative of a larger meridional gradient than in the present day. In the A1FI scenario, TGM concentrations in 2050 are projected to increase by 2.1–4.0 ng m^{-3} for the eastern US and 1.4–3.0 ng m^{-3} for the western US. This pattern corresponds to potential increases in wet deposition of 10–14 µg m^{-2} for the eastern US and 2–4 µg m^{-2} for the western US. The increase in Hg(II) emissions tends to enhance wet deposition and hence increase the risk of higher mercury entering the hydrological cycle and ecosystems. In the B1 scenario, mercury concentrations in 2050 are similar to present level concentrations; this indicates that the domestic reduction in mercury emissions is essentially counteracted by the effects of climate warming and emissions increases in other regions. The sensitivity analyses presented show that anthropogenic emissions changes contribute 32–53 % of projected mercury air concentration changes, while the independent contribution by climate change accounts for 47–68 %. In summary, global climate change could have a comparable effect on mercury pollution in the US to that caused by global emissions changes.

ACPD
13, 20165–20194, 2013

1 Introduction

The toxic effects of mercury (Hg) have been a serious concern to public health. Much scientific effort has been made to assess and monitor releases of mercury compounds and their effects on air quality (NADP, 1996; USEPA, 2006; Cohen et al., 2007; UNEP, 2008). Based on its toxicity and present pollution levels, the control of mercury emissions is an international priority (UNEP, 2008). Modeling future changes in pollutants is a useful method to support the formulation of pollution control strategies (Wang et al., 2008; Lei et al., 2012). Although many modeling studies have investigated past and present mercury pollutions (Bullock et al., 2002; Cohen et al., 2004; Selin et al., 2008; Lei et al., 2013b), potential changes in future levels of mercury compounds and their effect on air quality have not been well examined.

Climate and mercury emissions changes are major factors that affect the future atmospheric concentrations of mercury compounds. Changes in climate alone influence both the concentration and the future composition of atmospheric mercury. Owing to the low vapor pressure of mercury, the atmospheric lifetime and natural emissions of mercury are sensitive to climate change. Previous studies indicate that mercury emissions from soils are affected by changes in temperature and solar radiation (Lindberg et al., 1998; Zhang et al., 2001). Changes in general atmospheric circulation may also change the pathway of the atmospheric transport of mercury (Strode et al., 2008).

By contrast, changes in emissions also significantly affect the atmospheric concentrations of mercury compounds (Pan et al., 2010; Lin et al., 2011). The records from glacial ice cores in Wyoming (USGS, 2002) show that rising emissions are the primary factor behind the changes in atmospheric mercury concentration over past centuries. Modeling studies of preindustrial atmospheric mercury cycles also indicate that industrial emissions of mercury have changed the composition of atmospheric mercury (Selin et al., 2008; Holmes et al., 2010). Corbitt et al. (2011) found that emissions changes alone can significantly alter the source–receptor relationships for mercury following future emissions scenarios.

ACPD
13, 20165–20194, 2013

There are large uncertainties in future climate and mercury emissions, and these will impact future atmospheric mercury pollution (Pan et al., 2008). Recent studies strongly indicate that greenhouse gas emissions from human activities are the primary factor driving climate change over the past four decades (IPCC, 2001, 2007). Through the consideration of the uncertainties associated with future social and economic developments, the Intergovernmental Panel on Climate Change (IPCC) has developed a series of future emissions scenarios for projecting climate change over this century (IPCC, 2001, 2007; IPCC SRES, 2004). Many studies of future air quality changes have used these IPCC climate scenarios to assess the climate change impacts and analyze associated uncertainties (e.g., Wu et al., 2008; Pye et al., 2009; Lei et al., 2013a).

In addition, future emissions of mercury compounds are influenced by potential changes in social development as well as changes in climate. Mercury is emitted into the atmosphere from both anthropogenic and natural sources. Anthropogenic sources are closely associated with social and industrial developments. Anthropogenic emissions of global mercury were estimated to be 2190 Mg in 2000 (Pacyna et al., 2006). Streets et al. (2009) projected anthropogenic emissions of mercury to 2050 by considering different social development and energy use scenarios. Some natural emissions, including land and ocean emissions, are mostly affected by climate change. As a result, seasonal variations and spatial differences are significant. These characteristics of natural emissions reduce the effectiveness of the simple scaling method for future projections. Thus, the effects of climate change on natural emissions can only be considered by dynamic modeling methods (Poissant and Casimir, 1998; Zhang et al., 2001; Wängberg et al., 2001; Selin et al., 2008; Lei et al., 2013b).

In this study, a global 3-D atmospheric mercury model, termed the Community Atmospheric Model with mercury (CAM-Chem/Hg), is used to assess the effects of mercury on US air quality from 2000 until 2050. Three distinct climate/emissions pathways from the IPCC Special Report on Emissions Scenarios (SRES) are considered to address the uncertainties in future climate and full chemical emissions changes, including the A1FI, A1B and B1 scenarios representing the upper, middle and lower bounds of cli-

ACPD
13, 20165–20194, 2013

mate warming over the coming decades, respectively. Projections of anthropogenic mercury emissions in 2050 are based on the energy use assumed in the specific scenario, while natural emissions are projected through dynamic schemes for mercury emissions driven by future climate and environmental data. The analyses presented here examine both the individual and the combined effects of climate and mercury emissions changes on both surface mercury concentration and deposition over the US.

2 Model description

The model used in this study is a three-dimensional atmospheric mercury model based on the CAM-Chem climate-chemistry model. Details of the mercury model were previously described by Lei et al. (2013). The CAM-Chem model is run with fully coupled gas-aerosol phase chemistry, which is based on the chemical component of the Model of Ozone and Related Chemical Tracers (also known as MOZART) (Horowitz et al., 2003; Tie et al., 2001, 2005; Emmons et al., 2010; Lamarque et al., 2011; Lee et al., 2013). The mercury model can simulate three species of mercury in the atmosphere: elemental mercury (Hg(0)), divalent mercury (Hg(II)) and particulate mercury (PHg). To provide the best estimate of mercury emissions, a dynamic land mercury emissions scheme is used to calculate the emissions from soil, vegetation and reemissions that depend on the temperature, radiation and soil Hg storage. A simplified air–sea mercury exchange scheme is then used to calculate ocean emissions. Emissions from anthropogenic sources, biomass burning and volcanoes are also considered. The chemistry mechanism includes the oxidation of elemental mercury by ozone with temperature dependence as well as the oxidation by OH, H_2O_2 and chlorine in the gaseous phase. The aqueous reduction and oxidation of mercury species are also considered in the model. The computation of the transportation and deposition of mercury is finally merged into the original schemes for other chemicals in CAM-Chem.

ACPD
13, 20165–20194, 2013

In this study, the emissions of all chemical components used by the CAM-Chem model are projected to 2050. We first project emissions of chemicals other than mercury species from the 2000 to 2050 following the IPCC SRES, as previously carried out for the study of future ozone levels (Lei et al., 2012). Then, the anthropogenic emissions of mercury are projected to 2050 based on the energy use assumptions made in the IPCC SRES report (IPCC, 2001). The projections follow the IPCC A1FI, A1B and B1 scenarios and use the method introduced by Streets et al. (2009). Natural emissions from both land and ocean sources in 2050 are calculated using dynamic schemes built in the atmospheric mercury model (Lei et al., 2013b). Biomass burning in 2050 is also projected using the method introduced by Streets et al. (2009).

The CAM-Chem is driven by meteorological fields derived from the Community Climate System Model (version 3). The meteorology fields derived for the present atmosphere using this model are archived with 6 h temporal resolution, including winds, temperature, pressure, humidity and solar radiation. Simulations are performed with a 30 min time step and a horizontal resolution of 1.9° × 2.5° with 26 vertical levels from the surface (1000 hPa) to the 3-millibar level (~ 40 km altitude). Previous tests have demonstrated that roughly a 6 month spin-up is enough for CAM-Chem to minimize the influence of the initial conditions. In this study, each case was run for 5 yr (2048–2052) following a year of model spin-up. Unless noted otherwise, all results discussed are based on 5 yr averages. The modeled concentrations of mercury compounds were outputted at 1 h intervals.

3 Projection of future Hg emissions

The emissions of mercury compounds for 2050 are derived in three ways based on the source type and dynamic emissions approaches used in CAM-Chem.

ACPD
13, 20165–20194, 2013

3.1 Anthropogenic emissions

To examine the anthropogenic emissions of mercury in 2050, we use the projected results and scaling rates for the A1B and B1 scenarios presented by Streets et al. (2009). For the A1FI scenario, we project mercury emissions using the same method as deployed for calculating energy use information in the IPCC SRES A1FI scenario (RIVM, 2001). The A1FI scenario is characterized by the rapid increase in the consumption of fossil fuel energy and economic growth. We assume that no significant advance is made over the reported Hg removal levels in the A1FI scenario. The rates of the implementation of Flue Gas Desulphurization (FGD) by 2050 in coal-fired power plants for the A1 series scenarios are the same as referenced in RIVM (2001). Of the factors that affect mercury emissions, the use of coal, oil and natural gas in 2050 in the A1FI scenario is assumed to increase more than that in the A1B scenario. The final estimate of the amount of mercury emissions in each IPCC SRES region is calculated based on the FGD and the estimated energy growth in RIVM (2001). As introduced in Lei et al. (2013), we adopt the present (i.e., year 2000) anthropogenic emissions of mercury directly from those prepared by Pacyna et al. (2006). This emissions level is used as the base inventory to carry out the projection.

The resulting emissions inventories used in this study are summarized in Table 1. Global total Hg emissions are expected to increase in the future. Annual global mercury emissions in 2050 are projected in the range of 2390–5990 Mg, an increase of 9 % to 173 % over the total emissions in 2000. The main factor affecting Hg emissions is the increase in fossil fuel usage. Asia has the largest emissions increase, corresponding to its large population and rising energy demand.

Figure 1 shows the projected mercury emissions for North America. Total mercury emissions in 2050 increase to 305.7 $\mathrm{Mg\,yr^{-1}}$ in the A1FI scenario and to 225.9 $\mathrm{Mg\,yr^{-1}}$ in the A1B scenario, but decrease to 121.9 $\mathrm{Mg\,yr^{-1}}$ in the B1 scenario relative to the present value of 145.8 $\mathrm{Mg\,yr^{-1}}$. The most significant characteristic is that the amount and proportion of reactive mercury (Hg(II)) in total mercury emissions will increase,

ACPD
13, 20165–20194, 2013

whereas the proportion of elemental mercury (Hg(0)) will decrease by 2050 in all future scenarios. The global shares of primary emitted mercury species are 67 % for Hg(0), 25 % for Hg(II) and 7 % for PHg at present. These change in 2050 to 56 % for Hg(0), 40 % for Hg(II) and 4 % for PHg in the B1 scenario, to 47 %, 49 % and 4 % in the A1B scenario and to 49 %, 43 % and 8 % in the A1FI scenario. Owing to the implementation of FGD, this shift from Hg(0) (reduced) to Hg(II) (oxidized) may relatively reduce the long-range transport but significantly increase the local deposition of mercury.

3.2 Biomass burning and volcano emissions

Biomass burning emissions are specified as monthly means from the IPCC estimate of biomass burned and the IMAGE projection of managed forests for a typical year. The approach used and the Hg emissions factors as a function of vegetation types are adopted from Streets et al. (2009). The amount of open biomass burning is adopted from the IPCC (2001) projections, which are scenario-specific. Wildfire contribution to biomass emissions are estimated as a proportion of changes in mature forest area (IPCC, 2001; Streets et al., 2009). The IPCC projections of grassland and crop residue burning (human activities) are also used. The global estimated total mercury emissions from biomass burning for 2000 are 600 $Mg\,yr^{-1}$. This figure is projected to be 670 $Mg\,yr^{-1}$ in 2050 in the A1FI scenario, 570 $Mg\,yr^{-1}$ in 2050 in the A1B scenario and 447 $Mg\,yr^{-1}$ in 2050 in the B1 scenario. These estimates are comparable with previous results on present emissions or future projections of mercury emissions from biomass burning (Streets et al., 2001).

The volcanic emissions of mercury are estimated based on the sulfur emissions from volcanic sources in the Global Emissions InitiActive inventory. We use a Hg/SO_2 proportion of 1.5×10^{-6} for all volcanic eruptions (Aiuppa et al., 2007; Witt et al., 2008) in volcanic ash and the well-established SO_2 emissions (http://geiacenter.org) to indirectly calculate mercury emissions. A similar method has been used in previous studies (e.g., Ferrara et al., 2000; Nriagu et al., 2003; Pyle and Mather, 2003). The present estimate of mercury emissions from volcanoes is $\sim 500\,Mg\,yr^{-1}$. This value is considered

ACPD
13, 20165–20194, 2013

to be a historical average for the eruptions of active volcanoes and slow emissions from non-erupting stable volcanoes (http://geiacenter.org), and it is assumed to remain unchanged under future conditions.

3.3 Soil and ocean emissions

In order to project land and ocean emissions to 2050, we modify the dynamic emissions schemes for mercury developed in the CAM-Chem/Hg model (Lei et al., 2013b) in order to include the storage change in surface reservoirs. Surface Hg storage and climate are two of the major determining factors in Hg emissions. Storage change directly affects the amount of available mercury compounds. Climate change, especially changes in surface temperature, net solar radiation and surface wind, sensitively affect Hg emissions from land and oceans.

Surface storage change is related to the net deposition flux above the land and oceans. Anthropogenic and volcanic sources bring fresh mercury species into the biogeochemical cycle. Mercury storage in 2050 is determined by the net surface accumulations of fresh mercury in the past. Therefore, the change in surface Hg storage by 2050 should be the net accumulations of the fresh mercury emitted in future years before 2050. The latest estimate of present land mercury storage is around 240 000 Mg with a total deposition of 3260 $\mathrm{Mg\,yr^{-1}}$ and a total land emissions of 2900 $\mathrm{Mg\,yr^{-1}}$ (Smith-Downey et al., 2010). This estimation suggests a net new mercury increase in the surface land reservoir of 360 $\mathrm{Mg\,yr^{-1}}$, which accounts for 13 % of total net mercury emissions (anthropogenic + volcanic: 2770 $\mathrm{Mg\,yr^{-1}}$). Based on the CAM-Chem/Hg simulations, the estimate of a net increase in the atmospheric reservoir for the present atmosphere shows that around 1 % of newly emitted mercury will stay in the atmosphere. The rest (86 %) of the fresh mercury is deposited into the surface oceans. We assume that these partitioning ratios of new mercury are constant from 2000 to 2050. By using this linkage between surface Hg storage change and fresh mercury emissions, the dynamic emissions schemes in the CAM-Chem/Hg model can calculate future emissions fluxes.

ACPD
13, 20165–20194, 2013

The land emissions scheme is thus modified by considering a change in land mercury storage. The modified scheme is

$$F_2 = F_1 \exp\left[-1.1 \times 10^4 \left(\frac{1}{T_s} - \frac{1}{T_0}\right)\right] \exp\left[1.1 \times 10^3 \left(R_s - R_0\right)\right] \times C_i$$

where R_s is surface solar radiation and T_s is surface skin temperature. R_0 is the reference surface solar radiation with a value of 340 W m^{-2}. T_0 is the reference surface temperature with a value of 288 K. F_1 is the standard emissions dataset. C_i is the enrichment factor following each scenario. C_i is calculated as follow:

$$C_i = \frac{S_p + \alpha n \left(E_p + E_f\right)/2}{S_p}$$

where S_p is the present land storage of mercury (240 000 Mg). E_p is the present amount of total new mercury emissions. E_f is the projected amount of new mercury emissions. The value of α (0.13) is determined by the proportion of new mercury in the land reservoir. We assume that the net increase in new mercury follows a linear trend. The parameter n is the number of years relative to 2000. Here the value of n is 50.

The ocean emissions scheme is modified by considering the change in mercury concentration in the ocean mixing layer. The modified simple model is:

$$F = K_w \left(\left(C_w + m_i\right) - \frac{C_a}{H'}\right)$$

where m_i is the scenario-specific change in mercury concentration in the ocean mixing layer based on present-day values. Other variables and calculations follow Lei et al. (2013). As shown by Soerensen et al. (2010), 40 % of net deposition will enter the subsurface water that will not reemit into the atmosphere, while 60 % of the net deposition of new mercury will stay in the ocean mixing layer (Strode et al., 2007). m_i

ACPD
13, 20165–20194, 2013

is calculated by the following scheme:

$$m_i = \frac{60\,\% \frac{\beta n (E_p + E_f)}{2}}{71\,\% \times 4\pi R^2 \times d}$$

where β (0.86) is the proportation of new mercury in the surface ocean reservoir, which is estimated based on the present distribution of mercury deposition from anthropogenic sources. E_p is the present amount of total new mercury emissions. E_f is the projected amount of new mercury emissions. n is the number of years projected away from the present and R is the radius of the Earth. The factor 71 % accounts for the percentage of the Earth's surface covered by oceans. The parameter d is the depth of the ocean mixing layer. We set this to 50 m as an average depth and assume that Hg is evenly mixed in the ocean mixing layer (Sommar et al., 2010; Fisher et al., 2012).

4 Global mercury pollution in 2050

Figure 2 shows the global annual mean surface concentrations of total gaseous mercury (TGM) for the present day and for 2050 in the B1, A1B and A1FI scenarios. The changes in the spatial patterns of TGM show an overall worsening trend of mercury pollution following the increasing use of fossil fuel energy (B1 to A1FI), except for the US region in the B1 scenario. The result shows that the annual average TGM level by 2050 has increased by 10 % above the present level in the B1 scenario in which total global emissions increase in developing countries and decrease in developed countries. The temperature increase in scenario B1 is around 1 °C. A higher temperature will accelerate the mercury cycle and lead to more surface mercury being emitted into the atmosphere. The concentration increases in the A1FI and A1B scenarios are significant across the globe. The increases in Asia and Africa are especially large. The average concentrations over Asian industrial regions are above 6.0 ng m^{-3}. The TGM concentrations over the rest of the world also increase as a result of higher local emis-

ACPD
13, 20165–20194, 2013

sions and the enhanced long-range transport of mercury compounds from mercury emission industrial regions (Corbitt et al., 2011).

Figure 3 shows the zonal average of surface TGM concentrations for the present day and for 2050 according to these three scenarios. Generally, present and future zonal average concentrations have a similar spatial pattern. The zonal average concentration peaks at mid-latitudes of the Northern Hemisphere, where industrial sources are spreading. The average concentrations in the Southern Hemisphere are also maximized at the mid-latitudes. This result may be caused by the mining industries in the southern parts of Africa. The estimated mercury concentration in 2050 in the A1FI scenario shows a significant increase (up to 4.7 ng m^{-3}) in the middle and low latitudes. The peak value in 2050 is around twice as much as the present-day concentration. The peak value in the A1B scenario is around 0.5 ng m^{-3} lower than the peak value in the A1FI scenario. The concentration change in the B1 scenario in the middle and low latitudes is up to 0.5 ng m^{-3} higher than the present-day level. The concentration changes in the high latitudes are much smaller than those in the middle or low latitudes. At the high latitudes of the Southern Hemisphere, where fewer industrial and human activities occur, the average concentration change is as low as 0.2 ng m^{-3}.

5 Effect of mercury on US air quality

Atmospheric mercury concentrations in the US also change in these scenarios according to the model simulations. Figure 4 shows the annual average surface air concentrations of TGM for 2000 and 2050 in the B1, A1B and A1FI scenarios in the contiguous US. The spatial pattern of TGM concentrations exhibits higher values in the coastal area and the eastern US, where mercury-related industries are centered. The results show that the annual average TGM levels are projected to change little by 2050 in the B1 scenario as a result of the compensating effects of the emissions decrease and temperature increase of around 1 °C. Increased Hg emissions in neighboring countries may also contribute to the TGM concentration level seen for the US. By 2050 in the

ACPD
13, 20165–20194, 2013

A1B scenario, the annual average TGM level is projected to rise, with increases up to 1.4 ng m^{-3} over the eastern US. The TGM level in 2050 in the A1FI scenario shows the largest increases (up to 2.2 ng m^{-3}) in response to the largest rise in mercury emissions and the subsequent high degree of climate warming.

Figure 5 shows the simulated annual mean wet deposition of mercury in 2000 and 2050. Their spatial patterns are similar. Generally, the peak wet deposition region is the southeast, especially the coastal area of Georgia and South Carolina. This pattern is affected by the amount of precipitation and atmospheric concentration of mercury. The present annual wet deposition of mercury is above 12 µg m^{-2} for the eastern US and around 4 µg m^{-2} for the western US. By 2050 in the B1 scenario, the wet deposition only shows an increase of 1–2 µg m^{-2} for the eastern US, while there is little change for the western US. In the A1B scenario, the Midwest is projected to have a wet deposition of 18–24 µg m^{-2}, which is as strong as the present deposition in the southeast. The increase in the eastern US is around 6–12 µg m^{-2} compared with about 2–4 µg m^{-2} in the western US. The annual wet deposition in 2050 in the A1FI scenario increases by around 10–14 µg m^{-2} for the eastern US and around 2–4 µg m^{-2} for the western US.

6 Effects of climate change and anthropogenic emissions on US mercury levels

In order to understand how the changes in climate or anthropogenic emissions independently contribute to future changes in the concentrations of atmospheric mercury compounds, a series of sensitivity experiments, which incorporate climate change alone but keep emissions unchanged (i.e., the present-day level), are conducted for the three scenarios. The difference between these experiments and the present-day result represents the independent effect of climate change, while the difference between these experiments and future projections (climate plus emissions change results) for 2050 depicts the independent effect of anthropogenic emissions change.

For the projection of 2050 mercury effects considering both climate and anthropogenic emissions changes, Fig. 6 shows the simulated average concentrations of

ACPD
13, 20165–20194, 2013

annual mean surface mercury species over the continental US for 2000 and 2050 in the B1, A1B and A1FI scenarios. In the following analysis, the concentration unit is $ng\,m^{-3}$ for elemental mercury and $pg\,m^{-3}$ for reactive gaseous mercury and particulate mercury. The cylinder represents the average concentration over the US and the line shows the range (i.e., projected concentration range from minimum to maximum). As discussed in the previous section, the concentration of each mercury species increases in 2050. In the A1FI scenario, the increase is the greatest due to the large rise in anthropogenic emissions and high climate warming. Although elemental mercury remains the main chemical form of mercury in the atmosphere, the relative increase in the concentrations of reactive gaseous mercury is the largest in all three scenarios. This results from the increase in the emissions of reactive gaseous mercury and the accelerated oxidation of elemental mercury at a higher temperature.

Figure 7 shows the results for the sensitivity experiments of climate change alone, where anthropogenic emissions and land and ocean storages of mercury are all kept at the present-day level. Compared with the present-day concentration of each mercury species, the differences among the three scenarios are small. Table 2 summarizes the changes in the surface concentrations of Hg species over the US in 2050 caused by climate change or anthropogenic emissions changes. The average temperature increases in 2050 in the B1, A1B and A1FI scenarios are 1.0 °C, 1.4 °C and 1.7 °C, respectively. ΔHg shows the individual contribution of each factor to the average concentrations of mercury species in 2050. Climate change individually contributes to the surface concentration of elemental mercury $0.14\,ng\,m^{-3}$ in the B1 scenario, $0.45\,ng\,m^{-3}$ in the A1B scenario and $0.63\,ng\,m^{-3}$ in the A1FI scenario. By contrast, the contributions to concentrations of reactive gaseous mercury are $4.7\,pg\,m^{-3}$, $8.9\,pg\,m^{-3}$ and $11.6\,pg\,m^{-3}$ and those of particulate mercury are $3.3\,pg\,m^{-3}$, $6.8\,pg\,m^{-3}$ and $9.8\,pg\,m^{-3}$. The increase in temperature enhances emissions from land and ocean sources and accelerates the oxidation of elemental mercury. Therefore, both Hg(II) and PHg show relatively higher increases in concentration compared with Hg(0).

ACPD
13, 20165–20194, 2013

The effect of changes in anthropogenic emissions is calculated as the difference between the 2050 simulations with changes in climate plus emissions and the simulations with only climate change. The changes in anthropogenic emissions account for the increases in emissions due to the increased storage of mercury in land and ocean reservoirs, which mainly results from human activities. The decrease in anthropogenic emissions in the B1 scenario reduces the concentrations of elemental mercury by 0.04 ng m^{-3}, whereas the concentration of reactive gaseous mercury increases it by about 9.55 pg m^{-3}. The proportion of Hg(II) relative to total emissions also increases, resulting in a net rise in Hg(II) emissions in 2050 in the B1 scenario. The concentration of particulate mercury in 2050 is reduced by 0.6 pg m^{-3} in response to changes in anthropogenic emissions. In the A1B scenario, the change in the chemical partitioning of mercury emissions results in a significant shift from elemental mercury to reactive gaseous mercury in 2050. The contribution of changes in anthropogenic emissions to the concentration of elemental mercury is about 0.77 ng m^{-3}, while the contribution to Hg(II) is around 27.7 pg m^{-3} and that to PHg is around 2.1 pg m^{-3}. The contribution to Hg(II) is much higher than that at present. This trend continues in the A1FI case. In the A1FI scenario, the contribution of changes in anthropogenic emissions to the concentration of elemental mercury is about 1.05 ng m^{-3}, while it is 33.0 pg m^{-3} for Hg(II) and 8.0 pg m^{-3} for PHg.

7 Discussion and conclusions

We have investigated the effects of projected global changes in climate and emissions on atmospheric mercury and on air quality in the US by using a global atmospheric mercury model (CAM-Chem/Hg). Owing to projected future socioeconomic and technology development, developed countries show a slow increase or even a decrease in future levels of mercury emissions, while developing counties show an increasing trend. Total mercury emissions are expected to increase by 2050. Anthropogenic mercury emissions in 2050 range between 2386.2 Mg yr^{-1} and 5983.7 Mg yr^{-1}. For North

ACPD
13, 20165–20194, 2013

America, total anthropogenic emissions are possible to decrease. In all scenarios, the proportion of elemental mercury in emissions for 2050 decreases, while that of reactive gaseous mercury increases. Emissions from land and oceans in 2050 increase due to the accumulation of net mercury depositions in the surface storage reservoirs. With projected changes in biomass burning and wildfires, mercury emissions from the former are estimated to be between 447 $Mg\,yr^{-1}$ and 670 $Mg\,yr^{-1}$. These finding imply that industrial development will significantly affect global mercury pollution. Developing countries will be the main contributors to likely net global atmospheric mercury increases in the coming decades. Controlling the use of industrial materials that contain mercury compounds and improving technologies to reduce the release of mercury into the environment would thus be effective ways to mitigate mercury pollution.

For 2050, the zonal averaged concentration of surface TGM over the mid-latitude in the Northern Hemisphere shows a potential increase of 0.5–2.3 $ng\,m^{-3}$ above present levels. The zonal averaged concentration of surface TGM in the tropics and mid-latitudes in the Southern Hemisphere increase by about 0.5–1.2 $ng\,m^{-3}$. Changes in TGM concentrations at high latitudes are relatively small. This imbalanced change indicates that meridional transport of TGM from the relatively polluted low-mid latitude to the relatively clean high latitude will be stronger in 2050 than it is today.

Mercury's influence on air quality in 2050 over the continental US is examined by assessing the individual and combined effects of climate change and emissions changes. Climate change has a potential effect on the concentration of atmospheric elemental mercury of between 0.14 and 0.63 $ng\,m^{-3}$, while the effect on the concentration of reactive gaseous mercury is around 4.7–11.6 $pg\,m^{-3}$. Changes in anthropogenic emissions have relatively larger effects on mercury species over the continental US. The potential effect on the concentration of atmospheric elemental mercury is −0.04–1.05 $ng\,m^{-3}$, while the effect on the concentration of reactive gaseous mercury is around 9.55–33 $pg\,m^{-3}$. The impact of emissions changes is relatively more significant than that of climate change on future atmospheric mercury. As a result, the future TGM concentration may increase by 2.1–4.0 $ng\,m^{-3}$ for the eastern US and around 1.4–3.0 $ng\,m^{-3}$

ACPD
13, 20165–20194, 2013

for the western US in the A1FI scenario. Under the lower bound of potential climate warming (B1 scenario), TGM concentration does not see a significant change. The effect of climate change and remote emissions changes in surrounding areas is compensated by a domestic emissions decrease. This result indicates that climate change in the B1 scenario will have a comparable effect on US mercury pollution to emissions changes. Therefore, variation in mercury pollution is more sensitive to climate change than that for some other pollutants (e.g. surface ozone) which may be mainly affected by changes in anthropogenic emissions (Lei et al., 2013a). More effort therefore needs to be placed on monitoring toxic mercury pollution in the future.

We also analyzed the potential changes in wet deposition of mercury over the continental US and found that mercury wet deposition increased in all three scenarios. Precipitation change and an increase in Hg(II) concentration may increase the amount of wet deposition. Annual wet deposition in 2050 may increase by around 1–14 $\mu g\,m^{-2}$ for the eastern US and by around 0–4 $\mu g\,m^{-2}$ for the western US depending on projections in energy use. This result implies that more mercury from industrial emissions will be deposited into the water system and may further enter ecosystems. Thus, we could experience a further challenge in mercury contamination by mid-century.

Acknowledgements. The research was supported in part by the US Environmental Protection Agency Science to Achieve Results (STAR) Program under award number EPA RD-83337301. The research was also supported by the National Research Council (NRC) Associateship Awards. The authors acknowledge DOE/NERSC and NCSA/UIUC for the supercomputing support. We appreciate David Streets' work on Hg emission projection and Winston Luke's comments during the manuscript writing.

References

Bullock, R. and Brehme, K.: Atmospheric mercury simulation using the CMAQ model: formulation description and analysis of wet deposition results, Atmos. Environ., 36, 2135–2146, doi:10.1016/s1352-2310(02)00220-0, 2002.

ACPD
13, 20165–20194, 2013

Cohen, M., Artz, R., Draxler, R., Miller, P., Poissant, L., Niemi, D., Ratte, D., Deslauriers, M., Duval, R., Laurin, R., Slotnick, J., Nettesheim, T., and McDonald, J.: Modeling the atmospheric transport and deposition of mercury to the Great Lakes, Environ. Res., 95, 247–265, 2004.

Cohen, M., Artz, R., and Draxler, R.: NOAA Report to Congress: Mercury Contamination in the Great Lakes, Air Resources Laboratory, Silver Spring MD, Submitted to Congress on 14 May, 2007.

Cohen, M., Draxler, R., and Artz, R.: Modeling Atmospheric Mercury Deposition to the Great Lakes, Final Report for work conducted with FY2010 funding from the Great Lakes Restoration Initiative, NOAA Air Resources Laboratqory, Silver Spring, MD, 16 December, 2011.

Corbitt, E. S., Jacob, D. J., Holmes, C. D., Streets, D. G., and Sunderland, E. M.: Global source-receptor relationships for mercury deposition under present-day and 2050 emissions scenarios, Environ. Sci. Technol., 45, 10477–10484, 2011.

Emmons, L. K., Walters, S., Hess, P. G., Lamarque, J.-F., Pfister, G. G., Fillmore, D., Granier, C., Guenther, A., Kinnison, D., Laepple, T., Orlando, J., Tie, X., Tyndall, G., Wiedinmyer, C., Baughcum, S. L., and Kloster, S.: Description and evaluation of the Model for Ozone and Related chemical Tracers, version 4 (MOZART-4), Geosci. Model Dev., 3, 43–67, doi:10.5194/gmd-3-43-2010, 2010.

Ferrara, R., Mazzolai, B., Lanzillotta, E., Nucaro, E., and Pirrone, N.: Volcanoes as emission sources of atmospheric mercury in the Mediterranean basin, Sci. Total Environ., 259, 115–121, doi:10.1016/s0048-9697(00)00558-1, 2000.

Horowitz, L., Walters, S., Mauzerall, D., Emmons, L., Rasch, P., Granier, C., Tie, X., Lamarque, J.-F., Schultz, M., and Tyndall, G.: A global simulation of tropospheric ozone and related tracers: description and evaluation of MOZART, version 2, J. Geophys. Res., 108, 4784, doi:10.1029/2002JD002853, 2003.

Intergovernmental Panel on Climate Change (IPCC): Atmospheric chemistry and greenhouse gases, in: Climate Change 2001: The Scientific Basis, edited by: Houghton, J. T., Ding, Y., Griggs, D. J., Noguer, M., van der Linden, P. J., Dai, X., Maskell, K., and Johnson, C. A., Cambridge Univ. Press, New York, 239–288, 2001.

Intergovernmental Panel on Climate Change (IPCC): IPCC Special Report on Emissions Scenarios, Cambridge University Press, 2004.

Intergovernmental Panel on Climate Change (IPCC): IPCC Fourth Assessment Report: Climate Change 2007 (AR4), Cambridge University Press, Cambridge, UK and New York, NY, USA, 2007.

ACPD
13, 20165–20194, 2013

Lamarque, J.-F., Emmons, L. K., Hess, P. G., Kinnison, D. E., Tilmes, S., Vitt, F., Heald, C. L., Holland, E. A., Lauritzen, P. H., Neu, J., Orlando, J. J., Rasch, P. J., and Tyndall, G. K.: CAM-chem: description and evaluation of interactive atmospheric chemistry in the Community Earth System Model, Geosci. Model Dev., 5, 369–411, doi:10.5194/gmd-5-369-2012, 2012.

Lee, H., Olsen, S. C., Wuebbles, D. J., and Youn, D.: Impacts of aircraft emissions on the air quality near the ground, Atmos. Chem. Phys., 13, 5505–5522, doi:10.5194/acp-13-5505-2013, 2013.

Lei, H., Wuebbles, D. J., and Liang, X.-Z.: Projected risk of high ozone episodes in 2050, Atmos. Environ., 59, 567–577, doi:10.1016/j.atmosenv.2012.05.051, 2012.

Lei, H., Wuebbles, D. J., Liang, X.-Z., and Olsen, S.: Domestic versus international contributions on 2050 ozone air quality: how much is convertible by regional control?, Atmos. Environ., 68, 315–325, doi:10.1016/j.atmosenv.2012.12.002, 2013a.

Lei, H., Liang, X.-Z., Wuebbles, D. J., and Tao, Z.: Model analyses of atmospheric mercury: present air quality and effects of transpacific transport on the US, Atmos. Chem. Phys. Discuss., 13, 9849–9893, doi:10.5194/acpd-13-9849-2013, 2013.

Lin, C.-J., Shetty, S. K., Pan, L., Pongprueksa, P., Jang, C., and Chu, H.-W.: Source attribution for mercury deposition in the contiguous US: regional difference and seasonal variation, J. Air Waste Manage., 62, 52–63, 2011.

Lindberg, S., Hanson, P., Meyers, T., and Kim, K.-H.: Air/surface exchange of mercury vapor over forests – the need for a reassessment of continental biogenic emissions, Atmos. Environ., 32, 895–908, doi:10.1016/S1352-2310(97)00173-8, 1998.

National Atmospheric Deposition Program (NADP): Annual Data Summaries, available at: http://nadp.sws.uiuc.edu/lib/dataReports.aspx, 2008.

Nriagu, J. and Becker, C.: Volcanic emissions of mercury to the atmosphere: global and regional inventories, Sci. Total Environ., 304, 3–12, 2003.

Pacyna, E., Pacyna, J., Steenhuisen, F., and Wilson, S.: Global anthropogenic mercury emission inventory for 2000, Atmos. Environ., 40, 4048–4063, 2006.

Pan, L., Carmichael, G. R., Adhikary, B., Tang, Y., Streets, D., Woo, J.-H., Friedli, H. R., and Radke, L. F.: A regional analysis of the fate and transport of mercury in East Asia and an assessment of major uncertainties, Atmos. Environ., 42, 1144–1159, 2008.

Pan, L., Lin, C.-J., Carmichael, G. R., Streets, D. G., Tang, Y., Woo, J.-H., Shetty, S. K., Chu, H.-W., Ho, T. C., Friedli, H. R., and Feng, X.: Study of atmospheric mercury budget in East Asia using STEM-Hg modeling system, Sci. Total. Environ., 408, 3277–3291, 2010.

ACPD
13, 20165–20194, 2013

Poissant, L. and Casimir, A.: Water-air and soil-air exchange rate of total gaseous mercury measured at background sites, Atmos. Environ., 32, 883–893, 1998.
Pye, H., Liao, H., Wu, S., Mickley, L., Jacob, D., Henze, D., and Seinfeld, J.: Effect of changes in climate and emissions on future sulfate-nitrate-ammonium aerosol levels in the US, J. Geophys. Res., 114, D01205, doi:10.1029/2008JD010701, 2009.
Pyle, D. and Mather, T.: The importance of volcanic emissions for the global atmospheric mercury cycle, Atmos. Environ., 37, 5115–5124, 2003.
RIVM: The IMAGE 2.2 Implementation of the SRES Scenarios: A Comprehensive Analysis of Emissions, Climate Change and Impacts in the 21st Century, RIVM CD-ROM publication 481508018, National Institute for Public Health and the Environment, Bilthoven, the Netherlands, 2001.
Smith-Downey, N., Sunderland, E., and Jacob, D.: Anthropogenic impacts on global storage and emissions of mercury from terrestrial soils: insights from a new global model, J. Geophys. Res., 115, G03008, doi:10.1029/2009JG001124, 2010.
Soerensen, A., Skov, H., Jacob, D., Soerensen, B., and Johnson, M.: Global concentrations of gaseous elemental mercury and reactive gaseous mercury in the marine boundary layer, Environ. Sci. Technol., 44, 7425–7430, 2010.
Strode, S., Jaegle, L., Selin, N., Jacob, D., Park, R., Yantosca, R., Mason, R., and Slemr, F.: Air-sea exchange in the global mercury cycle, Global Biogeochem. Cy., 21, GB1017, doi:10.1029/2006GB002766, 2007.
Schroeder, W. H. and Munthe, J.: Atmospheric mercury – an overview, Atmos. Environ., 32, 809–822, 1998.
Selin, N., Jacob, D., Park, R., Yantosca, R., Strode, S., Jaegl'e, L., and Jaffe, D.: Chemical cycling and deposition of atmospheric mercury: global constraints from observations, J. Geophys. Res., 112, 1–14, doi:10.1029/2006JD007450, 2007.
Selin, N., Jacob, D., Yantosca, R., Strode, S., Jaegl'e, L., and Sunderland, E.: Global 3-D land-ocean-atmosphere model for mercury: present-day versus preindustrial cycles and anthropogenic enrichment factors for deposition, Global Biogeochem. Cy., 22, 1–13, doi:10.1029/2007GB003040, 2008.
Streets, D., Hao, J., Wu, Y., Jiang, J., Chan, M., Tian, H., and Feng, X.: Anthropogenic mercury emissions in China, Atmos. Environ., 39, 7789–7806, 2005.
Streets, D., Zhang, Q., and Wu, Y.: Projections of global mercury emissions in 2050, Environ. Sci. Technol., 43, 2983–2988, doi:10.1021/es802474j, 2009.

ACPD
13, 20165–20194, 2013

Tie, X., Brasseur, G., Emmons, L., Horowitz, L., and Kinnison, D.: Effects of aerosols on tropospheric oxidants: a global model study, J. Geophys. Res., 106, 22931–22964, 2001.
Tie, X., Madronich, S., Walters, S., Edwards, D., Ginoux, P., Mahowald, N., Zhang, R., Lou, C., and Brasseur, G.: Assessment of the global impact of aerosols on tropospheric oxidants, J. Geophys. Res., 110, D03204, doi:10.1029/2004JD005359, 2005.
UNEP Chemicals Branch: The Global Atmospheric Mercury Assessment: Sources, Emissions and Transport, UNEP-Chemicals, Geneva, 2008.
USEPA: EPA's Roadmap for Mercury, available at: http://www.epa.gov/hg/pdfs/FINAL-Mercury-Roadmap-6-29.pdf, last access: 1 March 2013, 2006.
USGS: Glacial Ice Cores Reveal A Record of Natural and Anthropogenic Atmospheric Mercury Deposition for the Last 270 Years, US Geological Survey, 2007.
Wängberg, I., Schmolke, S., Schager, P., Munthe, J., Ebinghaus, R., and Iverfeldt, A.: Estimates of air-sea exchange of mercury in the Baltic Sea, Atmos. Environ., 35, 5477–5484, 2001.
Wu, S., Mickley, L., Leibensperger, E., Jacob, D., Rind, D., and Streets, D.: Effects of 2000–2050 global change on ozone air quality in the US, J. Geophys. Res., 113, D06302, doi:10.1029/2007JD008917, 2008.
Zhang, H., Lindberg, S., Marsik, F., and Keeler, G.: Mercury air/surface exchange kinetics of background soils of the Tahquamenon River watershed in the Michigan Upper Peninsula, Water Air Soil Pollut., 126, 151–169, 2001.

ACPD
13, 20165–20194, 2013

Table 1. Anthropogenic emissions of Hg in 2000 and 2050 for each world region ($Mg\,yr^{-1}$) based on SRES scenarios.

Scenario	North American	Asia and Oceania	Europe and Mid East	Africa	Central and South America	World
2000[a]	145.8	1305.9	247.8	398.4	92.1	2189.9
2050 A1FI	305.7	3307.1	861.3	789.2	720.4	5983.7
2050 A1B[b]	225.9	2970.0	676.5	509.6	437.6	4855.6
2050 B1[b]	121.9	1208.9	358.1	357.0	340.4	2386.2

[a] Results from Pacyna et al., 2006.
[b] Projection results from Streets et al., 2009.

ACPD
13, 20165–20194, 2013

Table 2. Changes in surface concentrations of Hg species over the US in 2050 resulting from climate change and anthropogenic emission changes.

Scenario	ΔT	Effect of Change in	Hg Species	ΔHg (unit[a,b])
B1	+1.0 °C	Climate (Climate2050–Present)	Hg(0)	0.14
			Hg(II)	4.73
			PHg	3.3
		Anthropogenic Emission (2050–Climate2050)	Hg(0)	−0.05
			Hg(II)	9.55
			PHg	−0.6
A1B	+1.4 °C	Climate (Climate2050–Present)	Hg(0)	0.45
			Hg(II)	8.93
			PHg	6.8
		Anthropogenic Emission (2050–Climate2050)	Hg(0)	0.77
			Hg(II)	27.7
			PHg	2.1
A1FI	+1.7 °C	Climate (Climate2050–Present)	Hg(0)	0.63
			Hg(II)	11.6
			PHg	9.8
		Anthropogenic Emission (2050–Climate2050)	Hg(0)	1.05
			Hg(II)	33.0
			PHg	8.0

ΔT: Global Average Temperature Change in 2050 compared to 2000.
[a] Hg(0) in units of ng m^{-3}.
[b] Hg(II) and PHg are in units of pg m^{-3}.

ACPD
13, 20165–20194, 2013

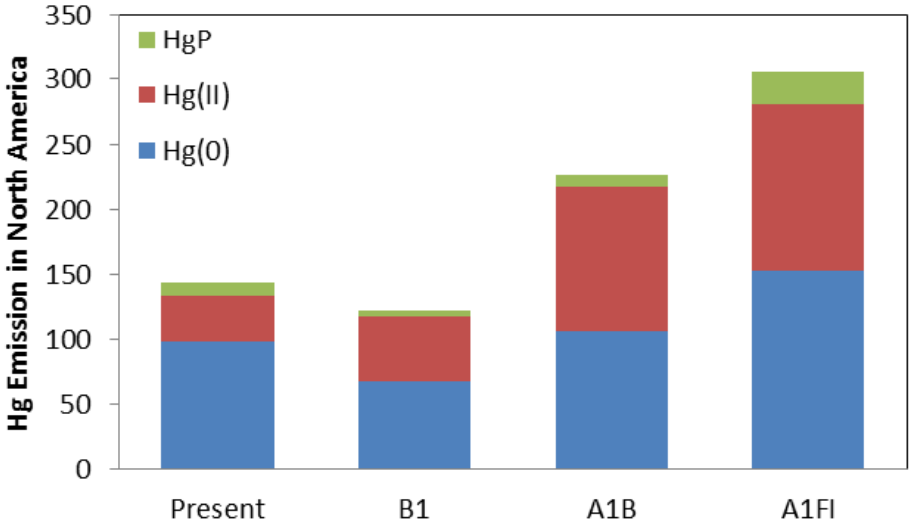

Fig. 1. Emissions of three mercury species for 2000 (present) and 2050 in North America (Units: tyr^{-1}). Emissions for 2050 are displayed in three future climate change scenarios: B1, A1B, and A1F1, representing the lower, middle and upper bounds of potential climate warming, respectively.

ACPD
13, 20165–20194, 2013

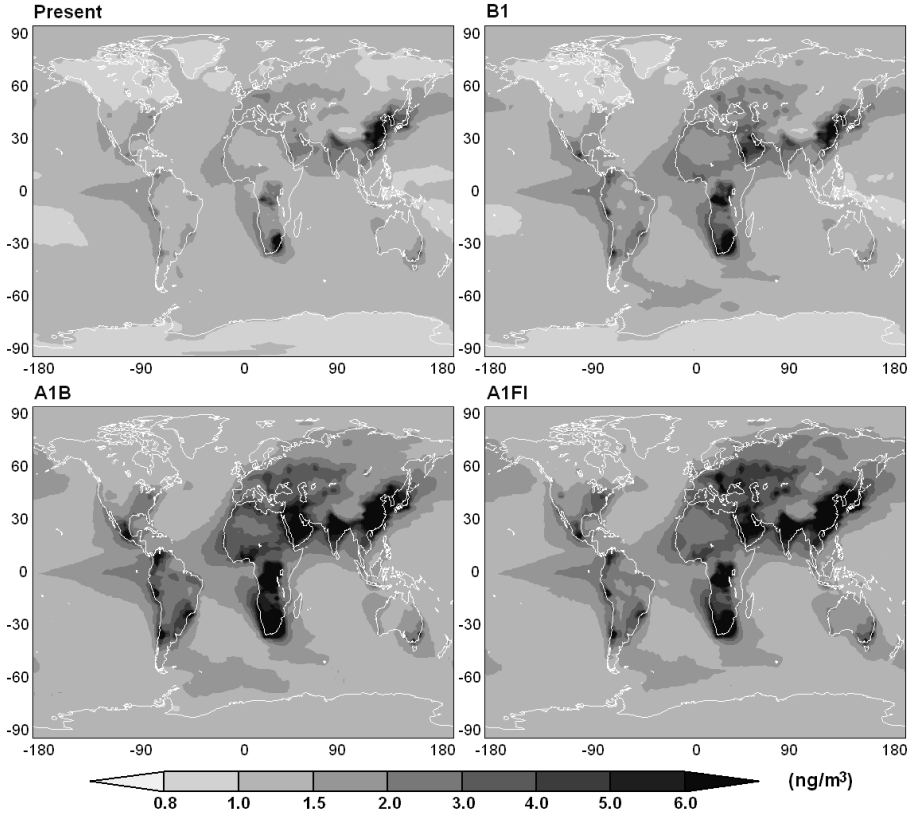

Fig. 2. Annual mean of global surface TGM concentrations for 2000 (present) and for 2050 under the B1, A1B and A1FI scenarios as simulated by the CAM-Chem/Hg model.

ACPD
13, 20165–20194, 2013

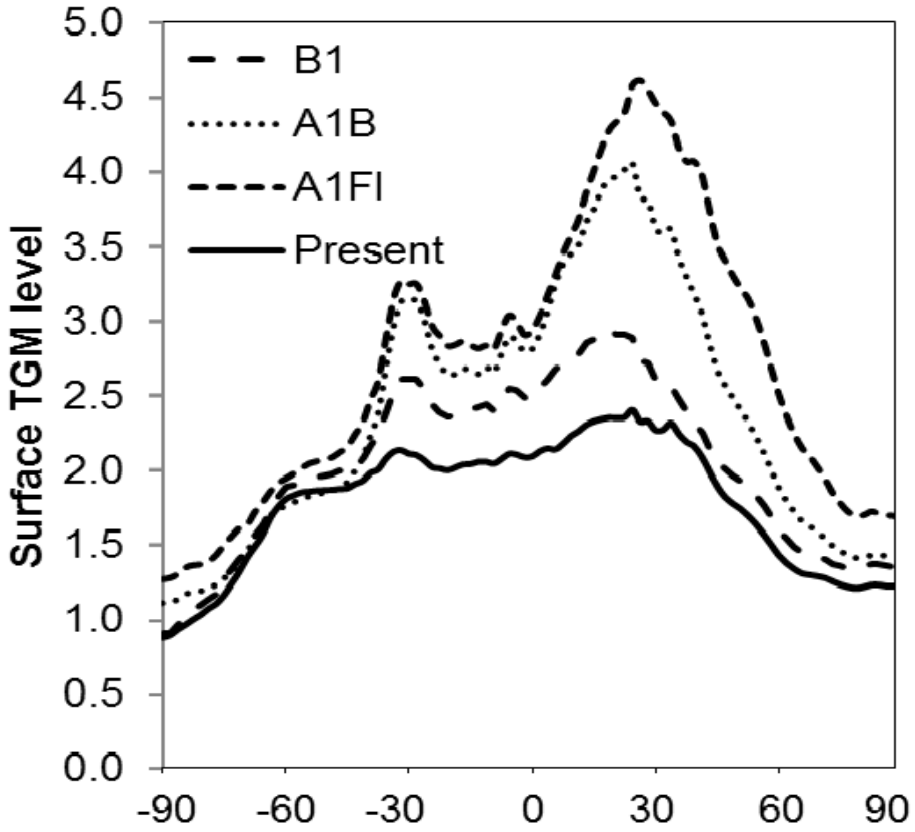

Fig. 3. Zonal averaged surface TGM concentrations for 2000 (present) and for 2050 under the B1, A1B and A1FI scenarios as simulated by the CAM-Chem/Hg model. (Units: ng m^{-3}).

ACPD
13, 20165–20194, 2013

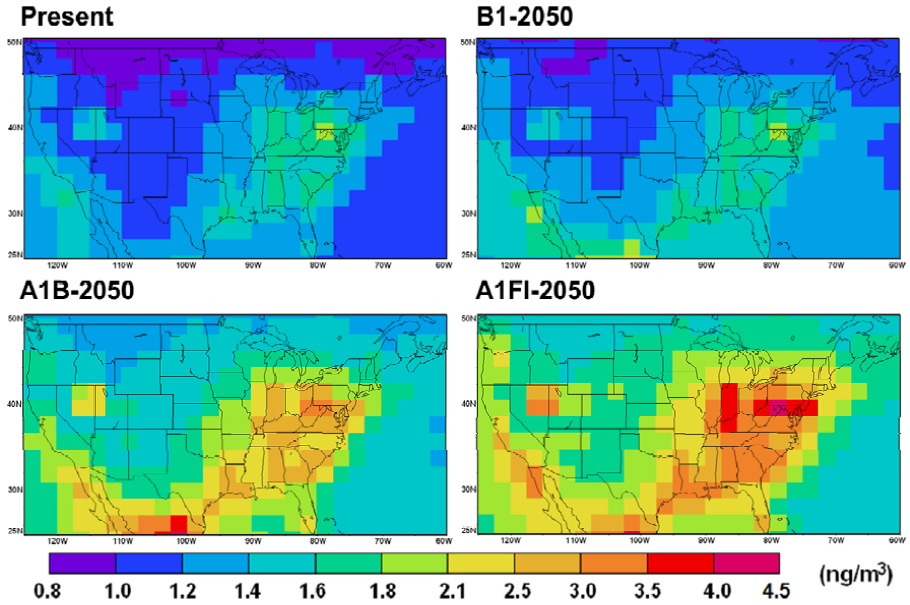

Fig. 4. Annual mean of simulated surface TGM concentrations over the continental US by CAM-Chem/Hg for 2000 (present) and for 2050 under the B1, A1B and A1FI scenarios.

ACPD
13, 20165–20194, 2013

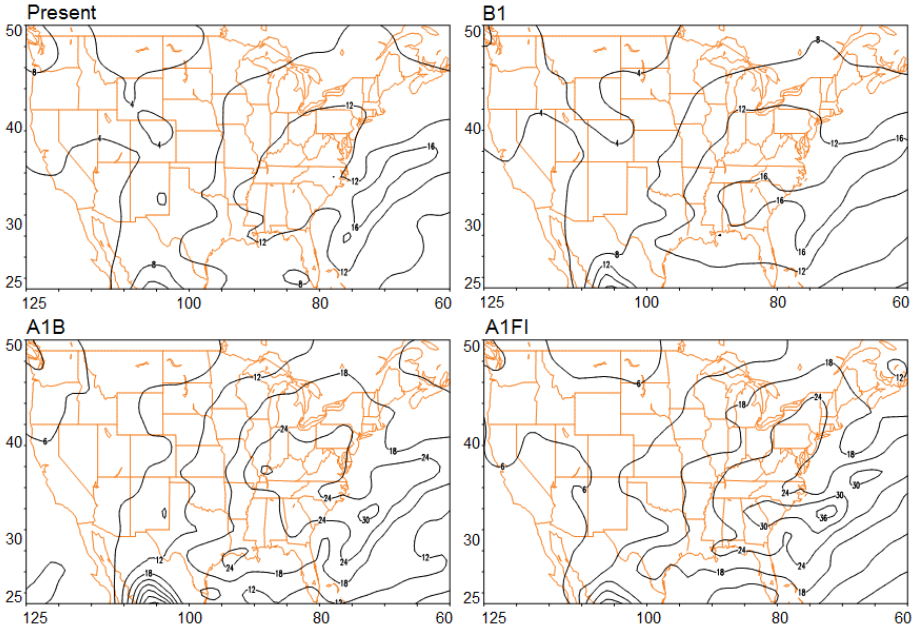

Fig. 5. Simulated annual mercury wet deposition for 2000 and for 2050 under the B1, A1B, and A1FI scenarios. (Units: $\mu g\,m^{-2}$).

ACPD
13, 20165–20194, 2013

Projections of atmospheric mercury levels and their effect on air quality

H. Lei et al.

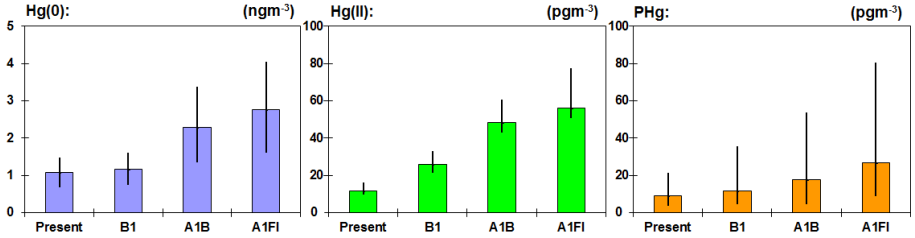

Fig. 6. Simulated annual mean concentrations of surface mercury species over the continental US for 2000 and for 2050 under the B1, A1B and A1FI scenarios considering both climate and emission changes. The columns show the averaged concentrations and the lines on the columns represent the range over the US.

ACPD
13, 20165–20194, 2013

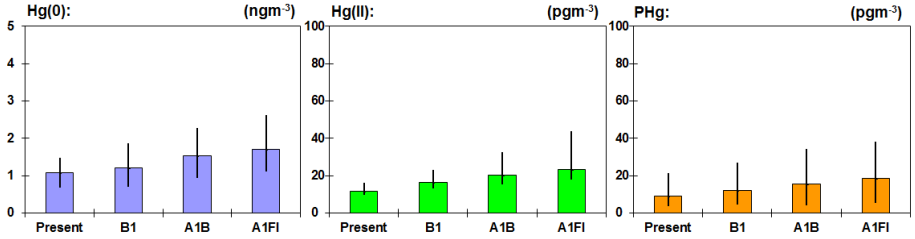

Fig. 7. Simulated annual mean concentrations of surface mercury species over the continental US for 2000 and for 2050 under the B1, A1B and A1FI scenarios considering climate change effects only. The columns show the averaged concentrations and the lines on the columns represent the range over the US.

ACPD
13, 20165–20194, 2013